

OAK RIDGE NATIONAL LABORATORY LIBRARIES



3 4456 0548327 8

3  
CENTRAL RESEARCH LIBRARY  
DOCUMENT COLLECTION

ORNL-3687  
UC-37 - Instruments  
TID-4500 (32nd ed.)

PERFORMANCE CHARACTERISTICS OF MODULAR  
NANOSECOND CIRCUITRY EMPLOYING  
TUNNEL DIODES

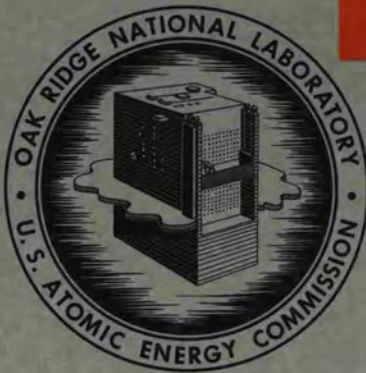
N. W. Hill  
R. J. Scroggs  
J. W. McConnell  
J. M. Madison

CENTRAL RESEARCH LIBRARY  
DOCUMENT COLLECTION

**LIBRARY LOAN COPY**

**DO NOT TRANSFER TO ANOTHER PERSON**

If you wish someone else to see this  
document, send in name with document  
and the library will arrange a loan.



**OAK RIDGE NATIONAL LABORATORY**

operated by

UNION CARBIDE CORPORATION

for the

U. S. ATOMIC ENERGY COMMISSION

Printed in USA. Price \$1.00. Available from the  
Office of Technical Services  
U. S. Department of Commerce  
Washington 25, D. C.

LEGAL NOTICE

This report was prepared as an account of Government sponsored work. Neither the United States, nor the Commission, nor any person acting on behalf of the Commission:

- A. Makes any warranty or representation, expressed or implied, with respect to the accuracy, completeness, or usefulness of the information contained in this report, or that the use of any information, apparatus, method, or process disclosed in this report may not infringe privately owned rights; or
- B. Assumes any liabilities with respect to the use of, or for damages resulting from the use of any information, apparatus, method, or process disclosed in this report.

As used in the above, "person acting on behalf of the Commission" includes any employee or contractor of the Commission, or employee of such contractor, to the extent that such employee or contractor of the Commission, or employee of such contractor prepares, disseminates, or provides access to, any information pursuant to his employment or contract with the Commission, or his employment with such contractor.

ORNL-3687  
Errata

PERFORMANCE CHARACTERISTICS OF MODULAR NANOSECOND  
CIRCUITRY EMPLOYING TUNNEL DIODES

N. W. Hill, R. J. Scroggs,  
J. W. McConnell, and J. M. Madison.

Please replace Fig. 19, page 16, of the subject report with the attached drawing. The page has been printed on gummed stock and may be pasted directly into the report.

Central  
Research Library  
Document Collection  
DEC 1 - 1964  
*pdl*

ORNL-3687

Contract No. W-7405-eng-26

Neutron Physics Division

PERFORMANCE CHARACTERISTICS OF MODULAR NANOSECOND  
CIRCUITRY EMPLOYING TUNNEL DIODES\*

N. W. Hill,\*\*, R. J. Scroggs,<sup>+</sup> J. W. McConnell,\*\*  
and J. M. Madison\*\*

OCTOBER 1964

\*Work supported by the National Aeronautics and Space Administration  
under NASA Order No. R-104.

\*\*Instrumentation and Controls Division, ORNL.

+Formerly of Instrumentation and Controls Division, ORNL; now with Oak  
Ridge Technical Enterprises Corp., Oak Ridge, Tennessee.

OAK RIDGE NATIONAL LABORATORY  
Oak Ridge, Tennessee  
operated by  
UNION CARBIDE CORPORATION  
for the  
U.S. ATOMIC ENERGY COMMISSION



3 4456 0548327 8

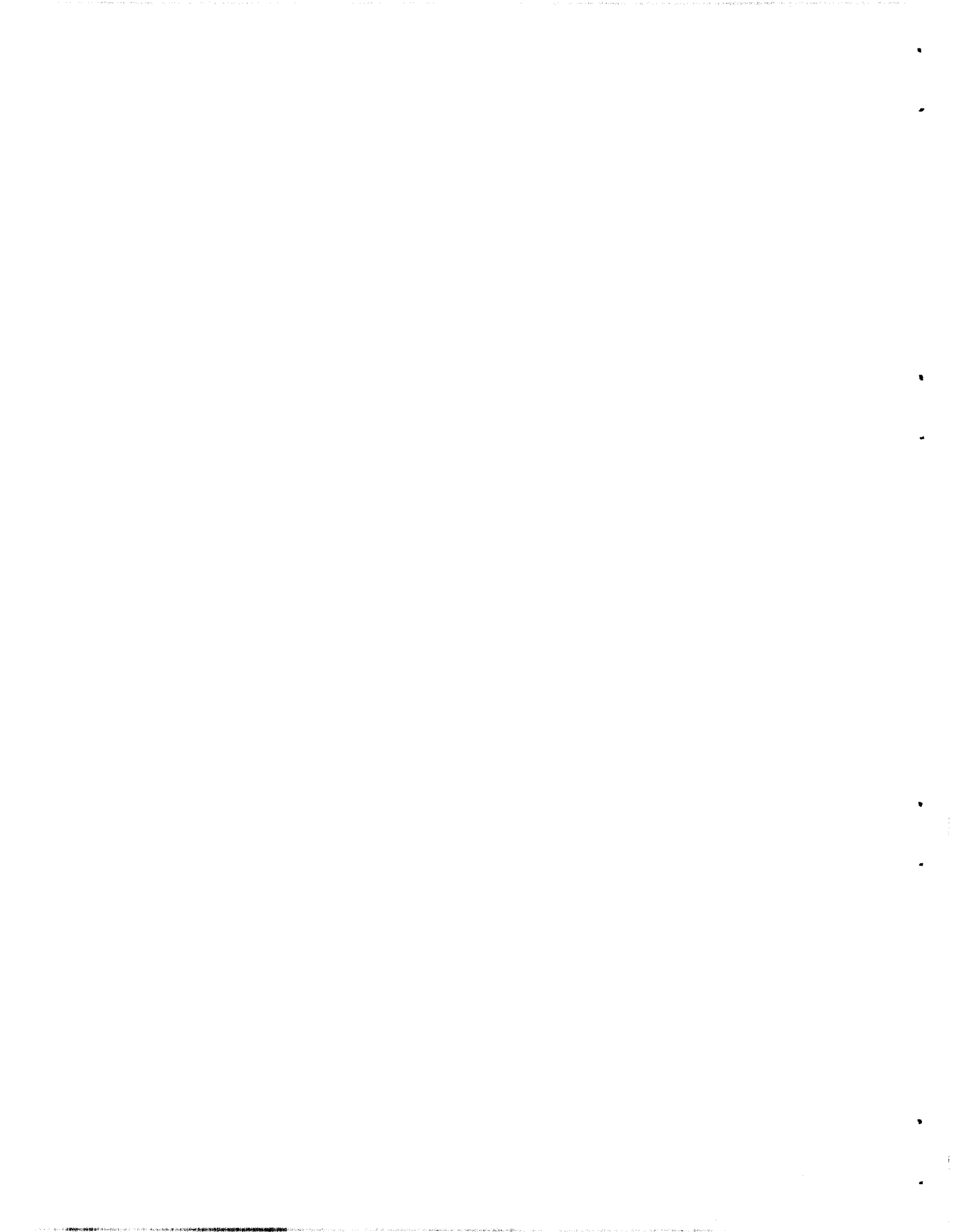


Table of Contents

	<u>Page No.</u>
Abstract -----	1
1. Introduction -----	2
2. Discriminator Modules -----	3
2.1. Slow-Recovery Discriminator Module -----	3
2.2. Fast-Recovery Discriminator Module -----	13
3. Coincidence and Anticoincidence Modules -----	21
3.1. Slow-Recovery Coincidence Module -----	21
3.2. Fast-Recovery Coincidence Module -----	23
3.3. Anticoincidence Module -----	23
4. Scaler-Driver Modules -----	23
4.1. Positive- and Negative-Output Scaler Drivers -----	23
4.2. 100-Mc Scaler Driver -----	27
5. Scaler Modifications -----	29
6. Power Supply Regulation -----	29
App. A. Construction Details -----	33

PERFORMANCE CHARACTERISTICS OF MODULAR NANOSECOND  
CIRCUITRY EMPLOYING TUNNEL DIODES

N. W. Hill,\* R. J. Scroggs,\*\* J. W. McConnell,\*  
and J. M. Madison\*

Abstract

Tunnel diodes have been used in the design and construction of a variety of modular circuitry used in instrumentation for high-energy particle experiments. Modules included fast- and slow-recovery discriminators, fast- and slow-recovery coincidence modules, positive- and negative-output scaler drivers, and a 100-Mc scaler driver. The individual univibrators used in the circuitry and the completed modules have been subjected to extensive tests to determine the effects of variations in operating temperature and in input pulse magnitude on resolution, pulse shape, walk, and thresholds.

It was found that circuitry using tunnel diodes is strongly affected by such variations, as well as by fluctuations in the power supply. It was also noted that parameter differences between supposedly identical tunnel diodes produced significantly large variations in module behavior.

It is concluded that the modular circuits discussed and shown in this report are satisfactory for their intended purposes, but that maximum performance and stability can be assured only by individual selection and testing of the tunnel diodes and by regulation of power supplies to +0.01% for both line and load.

An appendix gives some general details of the construction of the modules.

---

\*Instrumentation and Controls Division, ORNL.

\*\*Formerly of Instrumentation and Controls Division, ORNL; now with Oak Ridge Technical Enterprises Corp., Oak Ridge, Tennessee.

## 1. Introduction

Tunnel diodes, with their unique current vs. voltage response, have found wide application to high-speed (nanosec) switching and memory-sensing circuitry since their disclosure by Esaki in 1958.<sup>1-8</sup> They have recently been utilized in the construction of a variety of circuit modules included in the instrumentation of several high-energy particle experiments being performed by the ORNL Neutron Physics Division as part of its space-vehicle shielding studies.<sup>9</sup> These modules, which include circuits designed for pulse-height discrimination and for various coincidence and anticoincidence functions, were used in a gamma-ray spectrometer, in several proton-recoil telescopes, and for various purposes in particle time-of-flight measurements, as well as in a number of scaler-driver circuits.

Although tunnel diodes are known to have inherent high speed and to be operable over a wide range of temperatures, it was important for the applications noted above to obtain a detailed knowledge of the behavior of the several modules with variations in operating temperatures and magnitude of input signals. The present work is therefore primarily devoted to these subjects.

- 
1. L. Esaki, Phys. Rev. 108, 603 (1958).
  2. H. Ur, "Tunnel Diode High-Speed Circuits," Proceedings of the Berkeley Conference on Instrumentation for High-Energy Physics, IIa.2, 45 (1960).
  3. R. H. Bergman, IRE (Inst. Radio Engrs.) Trans. Electron. Computers, EC9(4), 430 (1960).
  4. G. Infante and F. Pandarese, "The Tunnel Diode as a Threshold Device: Theory and Application," Proceedings of the Conference on Nuclear Electronics, Belgrade (1961).
  5. A. L. Whetstone and S. Kounosu, Rev. Sci. Instr. 33, 423 (1962).
  6. A. L. Whetstone, IRE (Inst. Radio Engrs.) Trans. Nucl. Sci. 9, 280 (1962).
  7. M. J. Morgan, Semicond. Prod. 5(7), 9 (1962).
  8. M. Cooperman and R. H. Bergman, Electronics 36(28), 42 (1963).
  9. The assistance of W. H. Williams, W. H. Houston, and A. E. Ball, all of the Instrumentation and Controls Division, ORNL, in various phases of this work is gratefully acknowledged. The many helpful suggestions of R. W. Peelle, T. A. Love, and J. T. DeLorenzo are also acknowledged.

## 2. Discriminator Modules

Two basic discriminator modules were constructed. The first, the slow-recovery discriminator, was based upon a design by Whetstone<sup>6</sup> and, operating on pulses from a photomultiplier tube, performed the functions of low-level discrimination, pulse shaping, and "fan-out" for counting purposes. The second, the fast-recovery discriminator, was a modification of the slow-recovery discriminator to improve the pulse-pair resolution.

### 2.1. Slow-Recovery Discriminator Module

A diagram of the slow-recovery discriminator module is shown in Fig. 1. This circuit uses 10-mA gallium arsenide tunnel diodes having the typical current vs. voltage response shown in Fig. 2. The individual univibrators (broken lines in Fig. 1) have a dead time of 14 times the pulse width at half-height. Dead time is defined as the time separation between a pair of pulses that are just resolved when the second pulse has an amplitude 10% above threshold. The pulse width, and therefore the pulse-pair resolution, is dependent upon the capacitance of the diode, the resistive load ( $\sim 13\Omega$  in the diagram) and the value of the inductance L. Individual minimum thresholds are of the order of 50 mV; however, a TD-104 diode may be substituted for the XA650 in position 1 of Fig. 1 to give a threshold as low as 2 mV at this location. Figure 3 shows the output waveform of a typical univibrator used in the present work.

If it can be assured that all input pulses fall in an amplitude range from two to ten times threshold, dead time is significantly reduced. On the other hand, if the first pulse of an input pair is 100 times threshold and the second pulse 10% above threshold, dead time is about 30% greater than the 14X factor noted above. The pulse width for these univibrators is  $\sim 14$  nsec/ $\mu$ H for a wide span of inductance values, while the amplitude of the output pulse is constant for constant input amplitude for all values of the inductance above about 0.3  $\mu$ H. In this, as in most regenerative devices, there is an amplitude-dependent time delay or "walk" between the time the signal reaches the minimum triggering level and the time the discriminator fires. The delay is a function of the time required to charge the tunnel diode and stray capacitances, the pulse rise time,

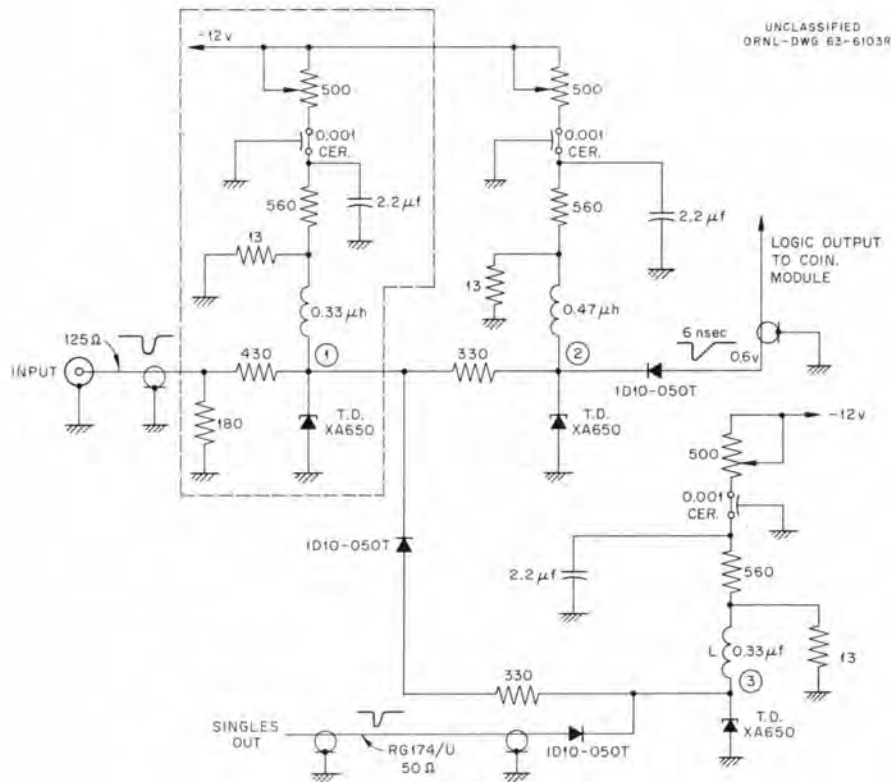


Fig. 1. Slow-Discriminator Module Circuit.

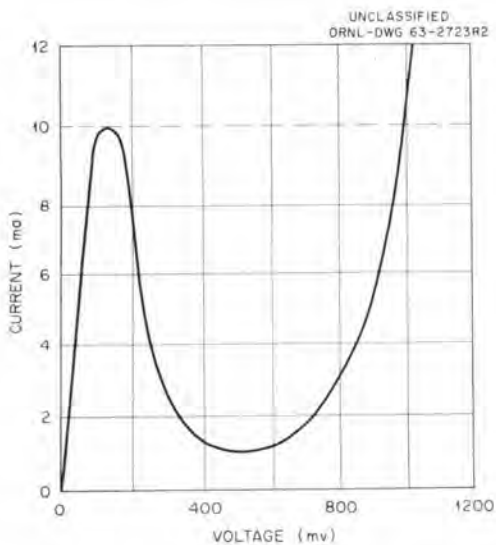


Fig. 2. Typical Current vs. Voltage Plot for a Tunnel Diode.

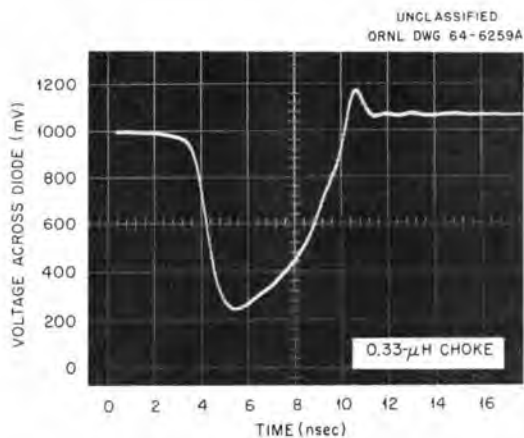


Fig. 3. Typical Univibrator Output Waveform.

and the percent of overdrive or pulse amplitude above threshold. The signal pulse rise time must be fast, not only to reduce the delay time but also because a shunt current path exists through the inductance L. The variation of delay time with input pulse amplitude is shown in Fig. 4, where the data are for a square input pulse with a rise time of less than 1 nsec and a duration of 35 nsec. The delay time decreases by about 4.5 nsec as the input pulse amplitude ranges from the half-fire threshold (100 mV) to 120 times threshold (12 V). The delay time was measured as the time between the 100-mV level of the driving pulse and the 100-mV level of the logic output. The walk from twice threshold to 120 times threshold is  $\sim 2.5$  nsec.

Other parameters of the discriminator modules are also adversely affected by input pulse amplitude, in particular the amplitude and width of the logic output pulse. As Fig. 5 shows, a factor of 120 increase in input pulse amplitude increased the output pulse width about 2.6 nsec or roughly 57%, while the amplitude of the output pulse increased 20% over the same range of input pulse amplitude.

In order to examine the behavior of the slow-recovery discriminator module as a function of temperature, a single module having resistors and capacitors temperature stable to 50 ppm/ $^{\circ}$ C was constructed. A measure of the difficulty in actually achieving the goal of temperature stability can be obtained from Figs. 6 and 7. Figure 6 shows the variation in the normalized peak current as a function of temperature for five germanium and five gallium arsenide diodes, while Fig. 7 shows the variation in the normalized peak voltage for the same ten diodes. Of the diodes tested, it appears that the gallium arsenide tunnel diode type TD-173 is the most nearly stable with temperature. However, individual TD-173's show considerable variation. Figure 8 shows tests of a single univibrator during which three TD-173's were interchanged. The curves for 69J and 89K have roughly the same shape and the threshold level decreases with increasing temperature, but in the case of diode No. 2K the threshold level steadily increases with temperature until approximate room temperature is reached, then drops slightly as the temperature is raised to  $\sim 50^{\circ}$ C.

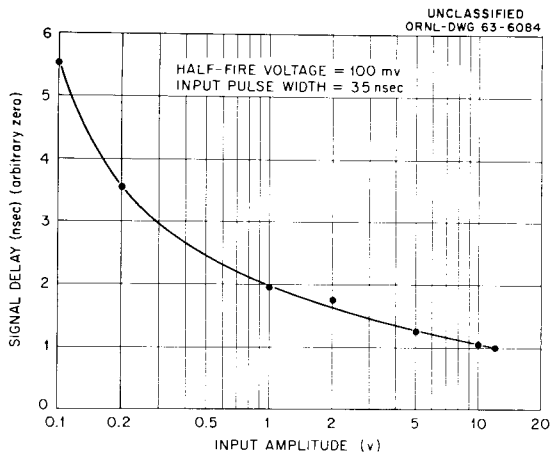


Fig. 4. Delay or Walk as a Function of Input Pulse Amplitude.

Fig. 5. Amplitude and Output Pulse Width of Discriminator Logic Output as Functions of Input Pulse Amplitude.

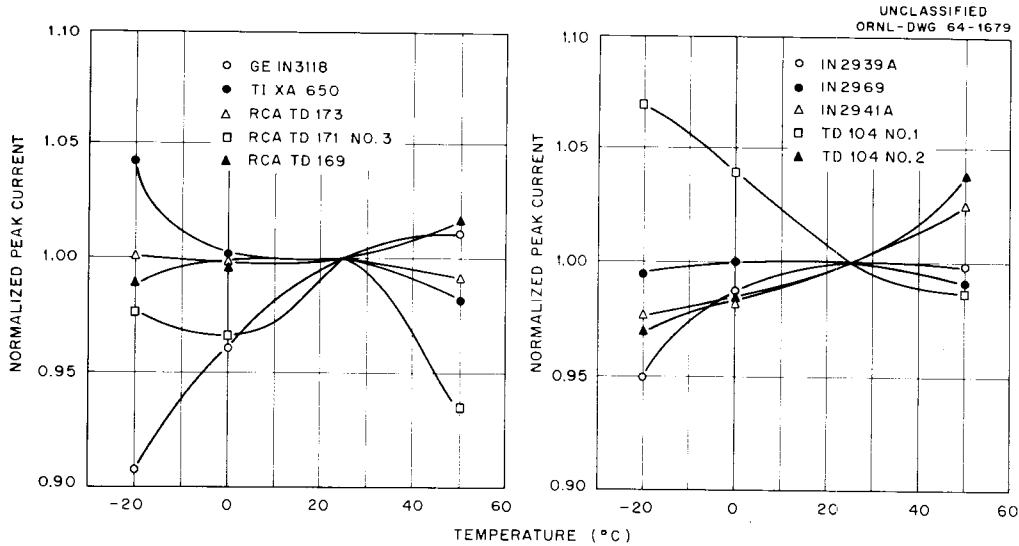
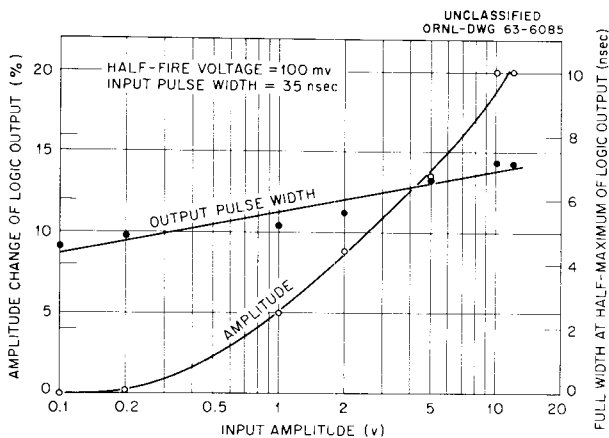


Fig. 6. Normalized Peak Current as a Function of Temperature; Germanium and Gallium Arsenide Diodes.

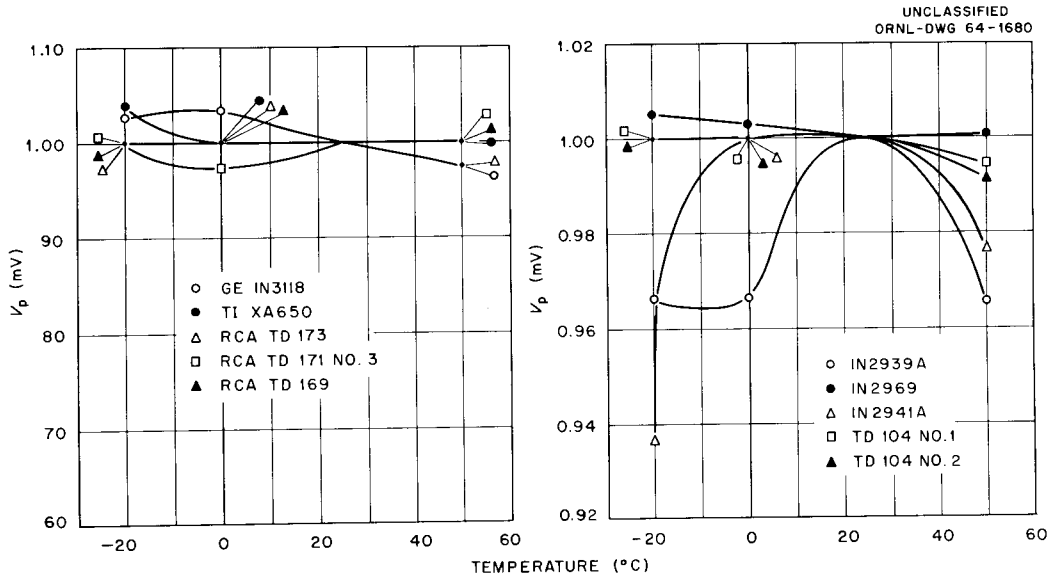


Fig. 7. Normalized Peak Voltage as a Function of Temperature; Germanium and Gallium Arsenide Diodes.

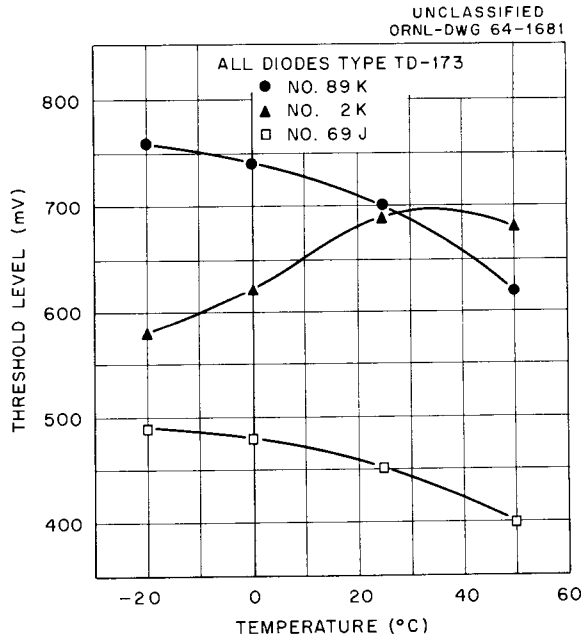


Fig. 8. Threshold Level as a Function of Temperature for a Single Univibrator.

Other basic parameters of the TD-173's tested also vary considerably among individual diodes. Figure 9 shows the variations in peak current as a function of temperature for the various diodes tested in a single univibrator. In this figure all data have been normalized to unity at 25°C. They show a difference depending on the individual diodes of from +5% to -3.2% at 0°C, and a difference of from -0.6% to -2.4% at 50°C.

Peak voltage as a function of temperature also varies widely between individual diodes of the same type, used in the same univibrator. Diode No. 69J, which produced the smallest shift in peak current with temperature, shows the greatest variation of peak voltage as shown in Fig. 10. It is clear from the evidence of these tests that the key to successful operation of modules employing these devices at present lies in individual testing and temperature compensation of the three diodes in each module.\*

The voltage-current characteristic curve for the TD-173 diodes used in the above tests can be closely approximated in the region of its peak by a parabola of the form

$$i = I_p \left( \frac{2v}{V_p} - \frac{v^2}{V_p^2} \right)$$

where

$i$  = current in the diode,

$v$  = voltage across the diode,

$I_p$  = the peak current,

$V_p$  = the peak voltage.

The d-c analysis of the univibrator, using the approximation given above to represent the diode, was performed to discover the shift of the d-c operating point with changes in  $I_p$  and  $V_p$ . Measured changes in  $I_p$

---

\*Note added in proof: Temperature-stable gallium arsenide and germanium diodes are reportedly now available, but the authors have not had the opportunity of testing them.

Fig. 9. Normalized Peak Current as a Function of Temperature for a Single Univibrator.

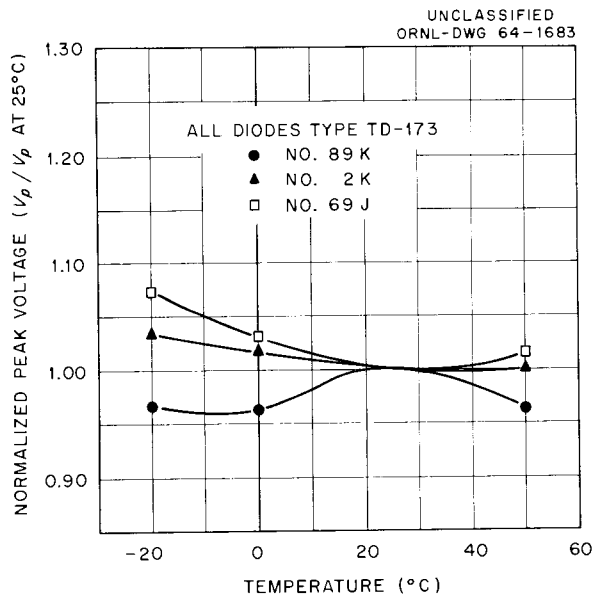
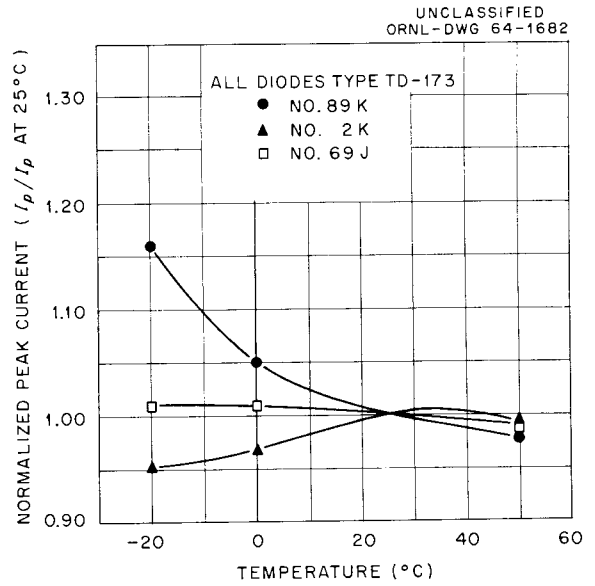


Fig. 10. Normalized Peak Voltage as a Function of Temperature for a Single Univibrator.

and  $V_p$  with temperature were used as input to predict the change in threshold level with temperature. For all three of the experimental diodes discussed above the direction of threshold change (increase or decrease) with temperature was correctly predicted, but the magnitude of the shift was always incorrect. The results lead to the surmise that the accuracy of the methods used to measure  $\Delta I_p$  and  $\Delta V_p$  as a function of temperature is inadequate, and to the suggestion that the possibility of a change in the a-c impedance of a tunnel diode with temperature should be investigated. Studies of the latter type are presently projected.

Figure 11 shows the variation of the half-fire threshold level with temperature for a discriminator module constructed of standard components (carbon resistors and non-temperature-stabilized ceramic capacitors). Over the range from 0 to 120°F, the half-fire threshold voltage decreases in a roughly linear fashion from 154.8 to 96.8 mV, about 37½%. Since in a practical sense temperature stability of the threshold level would be a very desirable attribute, the stability of the threshold was further studied by means of the module shown in Fig. 12. Because the method used to couple the output pulse of the discriminator diode to the other two univibrators influences the variation of the threshold, the alternative couplings shown in the figure were provided and tested. As Fig. 13 shows, the best temperature stability was achieved by diode coupling networks d and e (Fig. 12) to both the logic and the scaler-driver univibrators. This result, however, only applies when a particular set of diodes is used, and as Fig. 14 demonstrates, other sets of tunnel diodes can give different threshold level temperature coefficients. Interchanging the positions of the three diodes of a set can cause gross changes in the threshold level as a function of temperature, as is shown in Fig. 15. The results shown reinforce the conclusion that stable operation of the discriminator module can only be achieved by repetitious selection and testing of diodes until a suitable set is found.

The delay or walk associated with the half-fire point or threshold of a typical module appears essentially unaffected by temperature as shown by Fig. 16.

Fig. 11. Variation of Discriminator Threshold Level with Temperature.

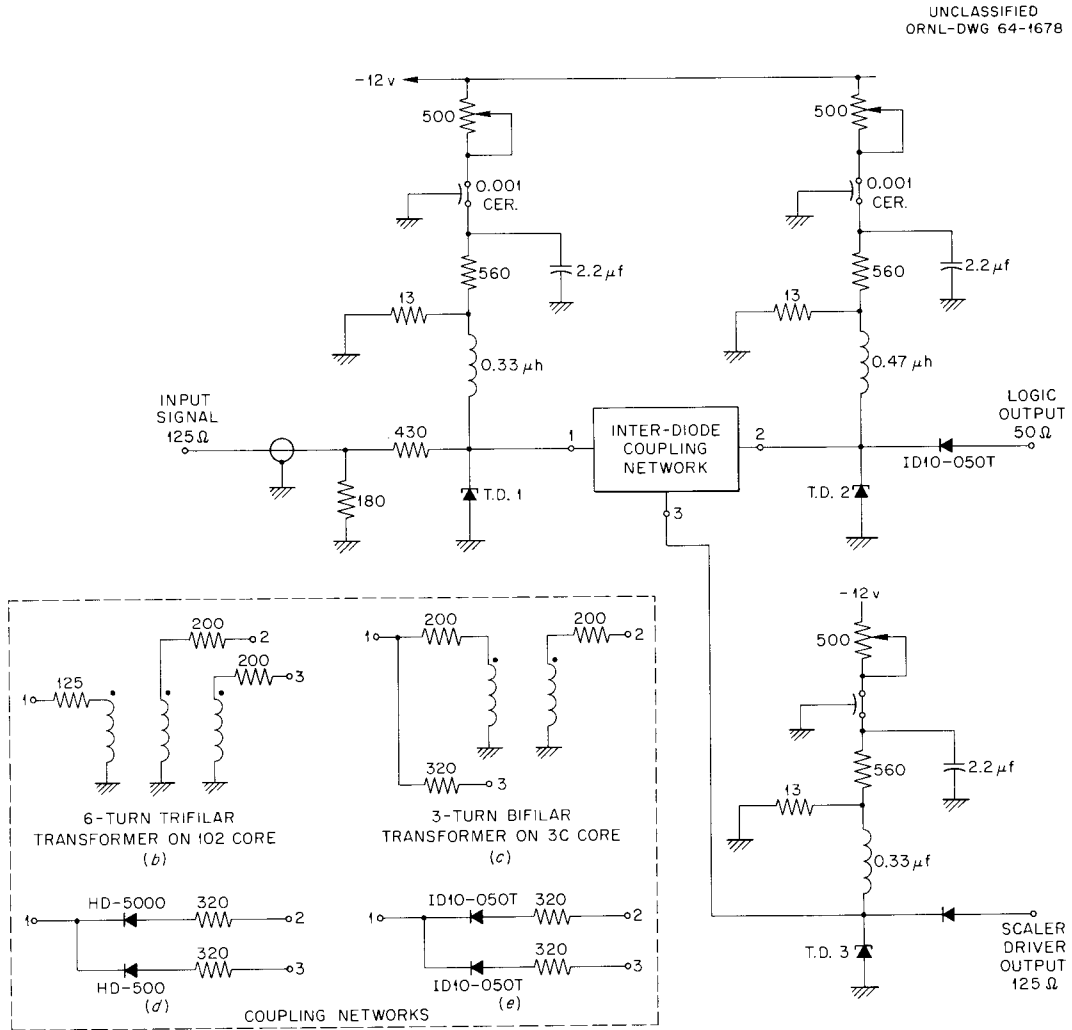
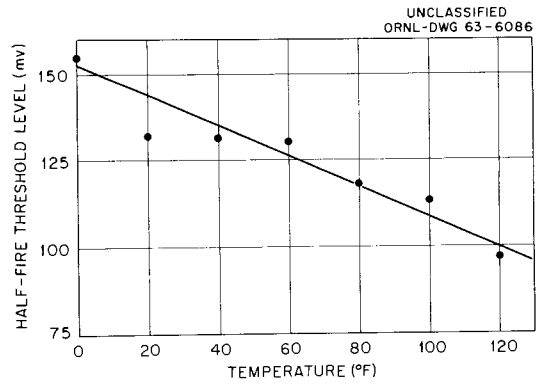


Fig. 12. Circuit Diagram of Test Module.

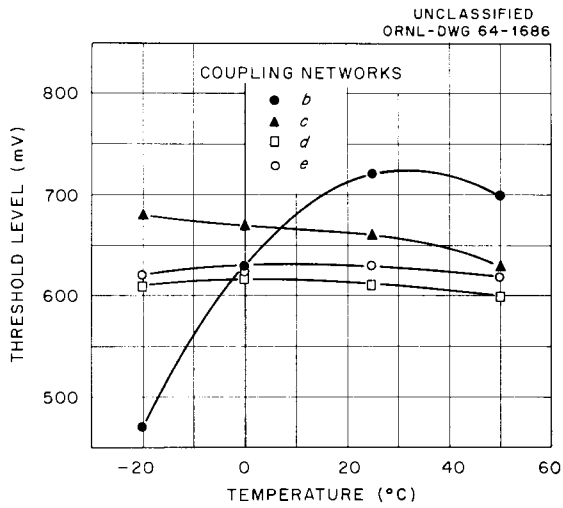


Fig. 13. Threshold Level as a Function of Temperature for Test Module with Various Coupling Circuits.

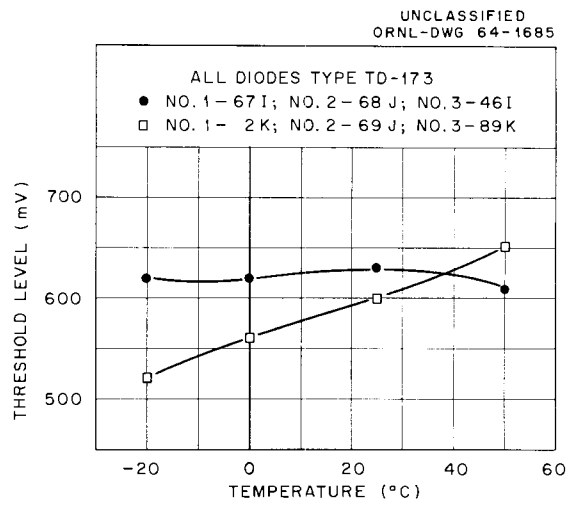


Fig. 14. Threshold Level as a Function of Temperature for Test Module, for Two Sets of Diodes.

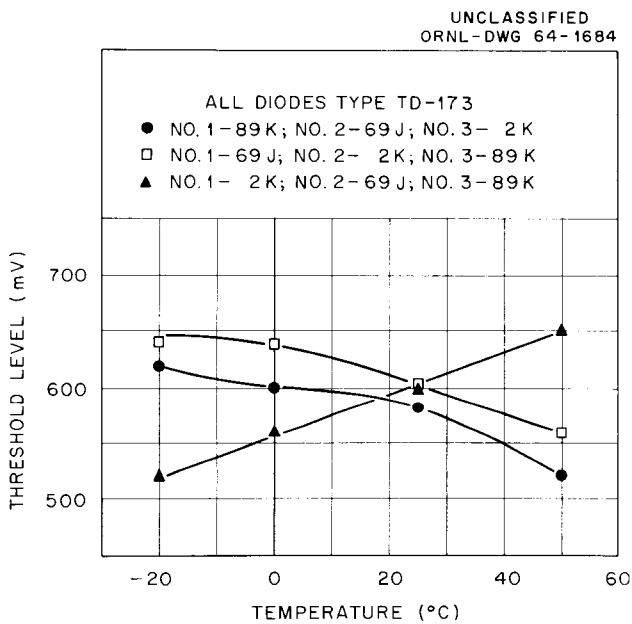
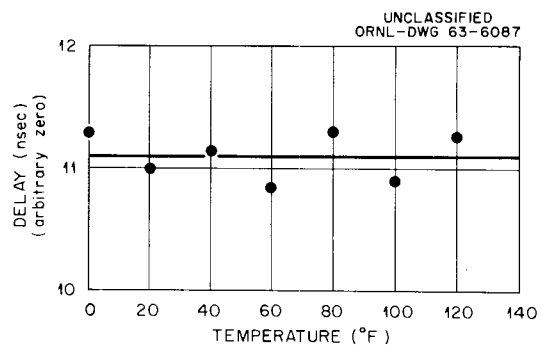


Fig. 15. Threshold Level as a Function of Temperature for Test Module; Diode Positions Interchanged.

Fig. 16. Delay of Half-Fire Output with Temperature. Input changed to give half-fire from logic output.



Although, as noted above, the pulse amplitude required to produce half-fire varies with temperature, the delay time after which the output occurs is constant if the pulse amplitude is adjusted to produce half-fire.

The effect of temperature variations upon the logic output of a non-temperature-stabilized slow-recovery discriminator is shown in the three parts of Fig. 17. As the temperature is increased from 0 to 120°F, the full width of the pulse at half maximum increases by roughly 5%, its amplitude increases by less than 6%, and the delay or walk associated with the pulse decreases by about 0.8 nsec. It is possible that the major portion of each of these variations is due to a changes in the threshold level, since the constant input amplitude of 200 mV used during these tests represents an overdrive factor of 2 at 120°F.

## 2.2. Fast-Recovery Discriminator Module

In many experiments the pulse-pair resolution given by the discriminator described above is inadequate. Although in principle the resolution is governed by the values of the loading resistor,  $R_L$ , and the inductance,  $L$ , in practice neither can be changed to improve the resolution significantly. Increases in  $R_L$  produce instability, while making  $L$  too small ( $< 0.3 \mu\text{H}$ ) not only reduces the amplitude of the output pulse but degrades sensitivity, especially to slowly rising pulses. "Nonlinear biasing," the substitution of a nonlinear load for the linear load  $R_L$  of Fig. 1, is, however, an excellent solution to the problem of improving resolution. Several slightly different nonlinear biasing elements have been proposed. The suggestions include common-base transistors,<sup>10,11</sup> tunnel rectifiers ("back" diodes),<sup>12</sup> germanium high-conductance diodes,<sup>13</sup> and tunnel-diode resistors.<sup>9</sup> All of these elements operate in a "clamping" mode once the tunnel diode has switched over its peak.

---

10. J. Amodei and W. F. Kosonocky, RCA Rev. 22, 669 (1961).

11. V. Radeka, Nucl. Instr. Methods 22, 153 (1962).

12. R. H. Bergman, M. Cooperman, and H. Ur, RCA Rev. 23, 152 (1962).

13. A. L. Whetstone, Rev. Sci. Instr. 34, 412 (1963).

A number of these nonlinear "clamps" were tested by operation in a high-speed univibrator. Tested were a 2N976 germanium transistor connected as a diode (collector and base connected together), a BD-503 gallium arsenide back diode, a Q3-100T germanium diode, an MA-4121 silicon diode, and common-base transistors (2N976 and 2N955). Figure 18 shows the characteristic current vs. voltage curves of the 2N976, BD-503, Q3-100T, and MA-4121 elements. The characteristic curve of the 2N976, with its flat plateau, sharp shoulder, and nearly vertical descent most nearly approaches the ideal behavior for a nonlinear biasing application, and since the 2N976 also met specifications of economy, dependability, and simplicity of utilization, it was chosen for nearly exclusive use. A diagram of a typical high-speed discriminator module is shown in Fig. 19.

Nonlinear biasing is compared with linear biasing in Fig. 20, where the biased element is a 10 mA gallium-arsenide tunnel diode. It is apparent that the 2N976 clamp has a comparatively high resistance for all low-voltage tunnel diode bias states and for the time when the tunnel diode is switching over the peak, and less resistance than the linear load after switching. Thus the transistor clamp is a high-impedance shunt path before and during switching and therefore the univibrator requires much less input current, making it more sensitive to slow rise-time and d-c inputs. Since the voltage across the inductance,  $V_L$ , is much larger than it is with the linear load, the time required for recovery to the original bias point is much less with the transistor load, and because of the more nearly ideal switching characteristics of the transistor, the recovery time is more clearly defined. When the univibrator is in its high-voltage state, where  $V_L$  is much smaller for the nonlinear load, the recovery time and therefore the output pulse width is longer for a given value of  $L$ ; thus the nonlinear load provides faster recovery for a wider pulse. The sensitivity achieved for weak triggering pulses, however, is about one-fourth that of the slow discriminator (see table at end of this section). This disparity has been reported<sup>13</sup> to disappear when the value of  $L$  is raised above 0.5  $\mu\text{H}$ . The difference in sensitivity is reduced to a factor of 2 by the use of high-beta 2N976 transistors.

Since the nonlinear load results in recovery times shorter than 10 nsec, care must be exercised to ensure that broad input pulses, especially

Fig. 17. Variation of Delay, Logic Output Pulse Amplitude, and Output Pulse Width with Temperature.

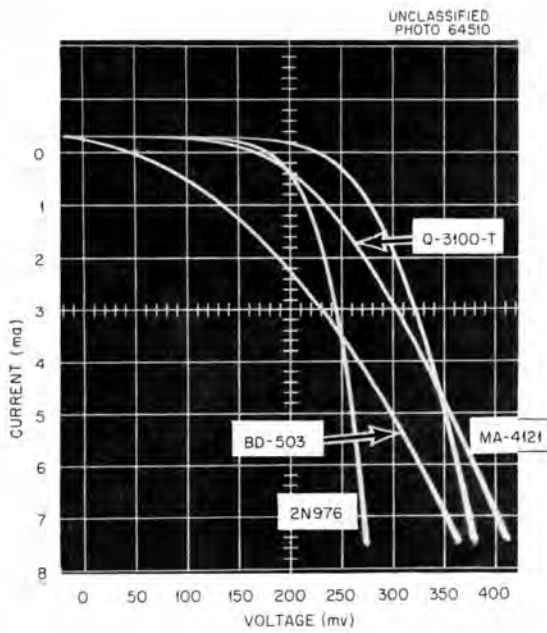
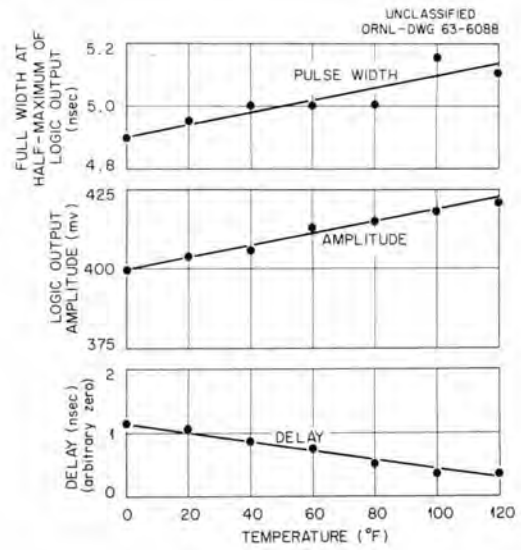


Fig. 18. Current vs. Voltage Characteristic for Several Nonlinear "Clamping" Devices (2N976 Used as a Diode).

UNCLASSIFIED  
ORNL-DWG 63-6089R

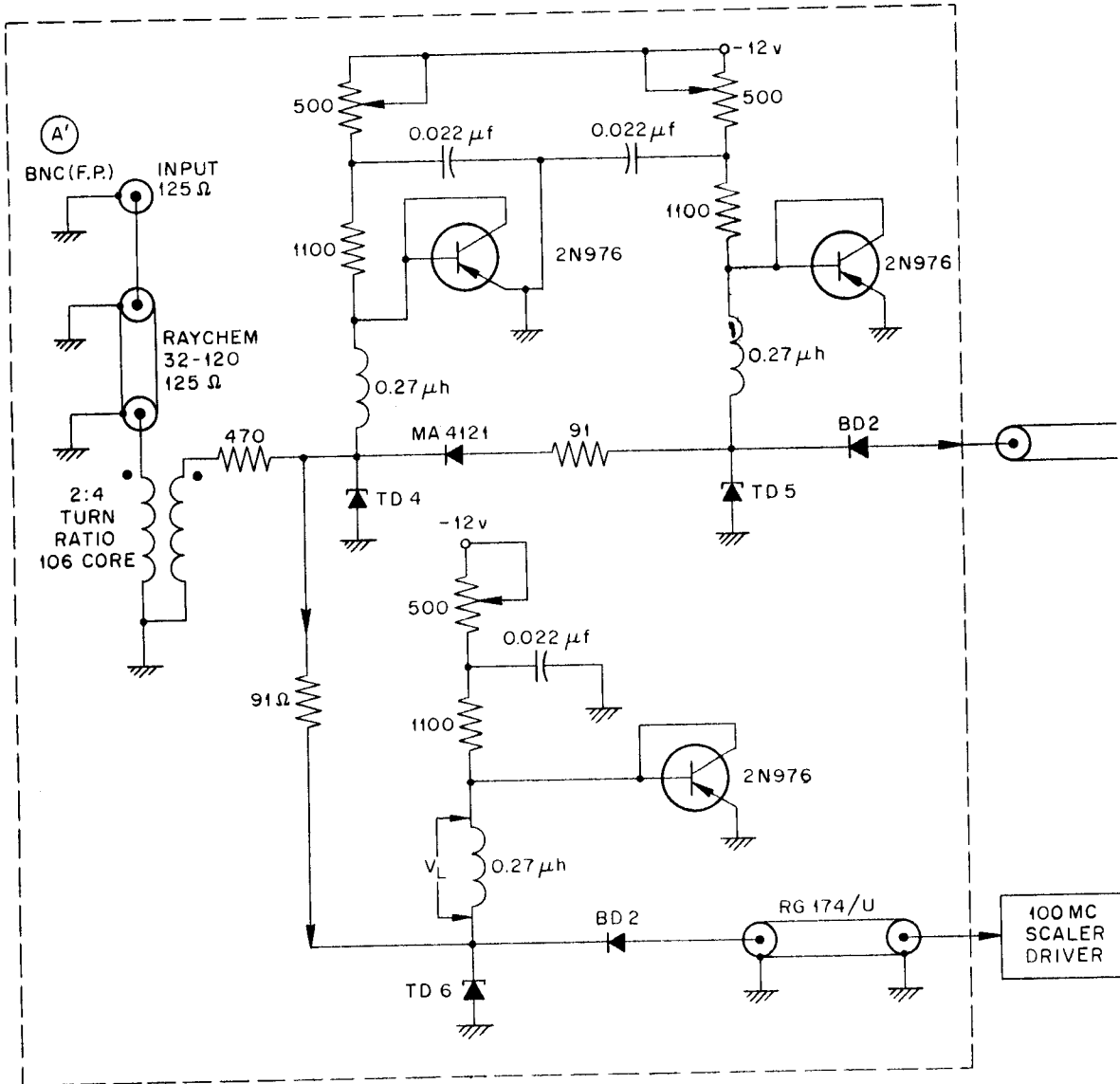


Fig. 19. High-Speed Discriminator Module Circuit.

from overloads, do not induce multiple pulsing. In the circuit shown in Fig. 19, the termination of the 125- $\Omega$  input by the 2:4 ratio transformer reduces such multiple pulsing, but at some sacrifice in sensitivity. The low-frequency response of the transformer is insufficient to couple the slower components of the input pulses.

Some aspects of the variation in the response of the fast-discriminator module with temperature have been examined. The half-fire threshold as a function of temperature is shown in Fig. 21. The drop in threshold level is about 100 mV, in comparison with the 58 mV of the slow discriminator. Recalling, however, the strong dependence of the threshold level upon the individual diode characteristics, it is reasonable to expect that much or all of the difference between 100 and 58 mV is due to parameter differences between diodes.

As was true for the slower module, the delay or walk for the fast-recovery discriminator does not appear to be a function of temperature as shown in Fig. 22. For these data the input was adjusted to produce half-fire at each temperature.

The logic output pulse amplitude of a typical fast-recovery discriminator as a function of temperature is shown in Fig. 23. Over the 120°F range the pulse amplitude decreases by about 11%, when measured with the coupling diode, BD2, in series.

The effects produced at the logic output of the fast-recovery discriminator due to an increase in the input pulse amplitude are shown in Fig. 24. The total delay change for inputs 1.25 times threshold (500 mV) to 15 times threshold (6 V) is 2.9 nsec, while over the range from 2 to 15 times threshold the total change is  $\sim 1$  nsec. These times are comparable to those obtained with the linearly loaded discriminator. The pulses used in the comparison had rise times of  $< 1$  nsec. The amplitude stability with overdrive for the fast-recovery discriminator, however, is somewhat poorer than that of the slower model, a result explained by the lower values of coupling resistances used between univibrator stages in the fast module. Output pulse width of the fast-recovery discriminator remains essentially constant for input amplitudes of from 0.5 to 4 V, becoming slightly broader for inputs of from 4 to 10 V.

UNCLASSIFIED  
ORNL-DWG 63-6090R

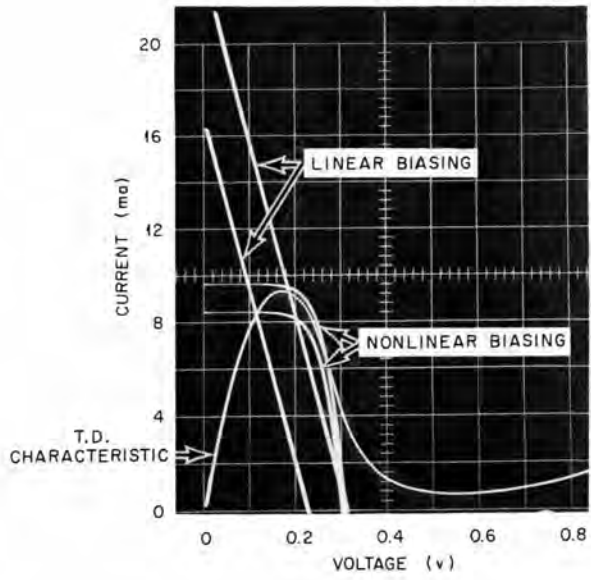
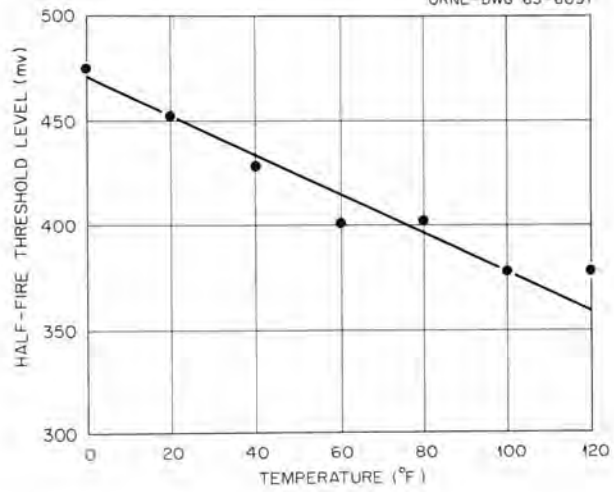


Fig. 20. Current vs Voltage Curves for Linear and Nonlinear Discriminator Biasing.

Fig. 21. Half-Fire Threshold Stability with Temperature for Nonlinearly Biased Discriminator.

UNCLASSIFIED  
ORNL-DWG 63-6091



UNCLASSIFIED  
ORNL-DWG 63-6092

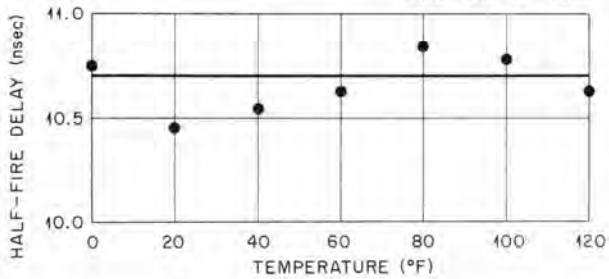
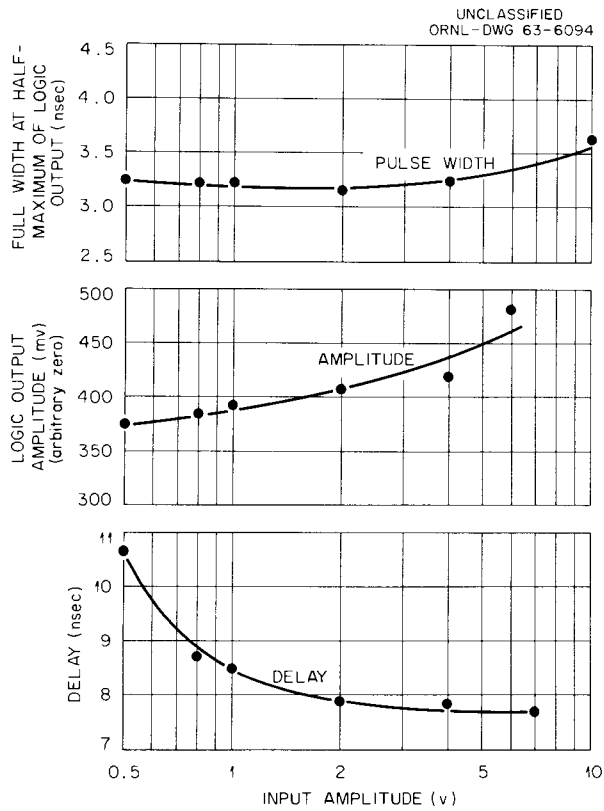
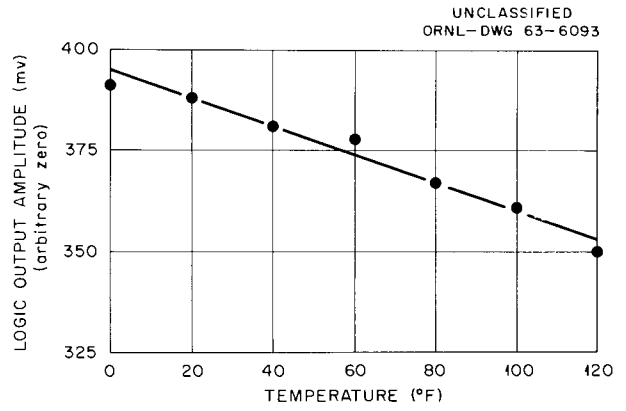


Fig. 22. Delay of Half-Fire Point vs Temperature for Nonlinearly Biased Discriminator.

**Fig. 23. Logic Output Amplitude Stability with Temperature for Nonlinearly Biased Discrimination.**



**Fig. 24. Effects of Input Pulse Amplitude on Delay, Amplitude, and Pulse Width of Logic Output Pulse from Nonlinearly Biased Discriminator.**

Performance data for the fast-recovery discriminator are tabulated and compared with parallel data for the slow-recovery discriminator in Table 1.

Table 1. Comparison of Performance Data: Slow-Recovery Discriminator Module vs. Fast-Recovery Discriminator Module\*

	Slow-Recovery Discriminator	Fast-Recovery Discriminator
Input Pulse Data		
Threshold:		
Amplitude (mV)	50	120
Amplitude Shift with Temperature (mV/°F)	- 0.5	- 0.83
Width (nsec):		
L = 0.33 $\mu$ H	4.2	4.6
L = 0.27 $\mu$ H		3.8
Width (nsec/ $\mu$ H)	~ 13	~ 14
Pulse-Pair Resolution (nsec):		
Input Amplitude 1.10X Threshold	55	15
Input Amplitude 2X Threshold	41	12
Input Amplitude 3X Threshold	39	10
Output Pulse Data		
Delay Change with Input Amplitude Change (nsec)		
Threshold to 120X Threshold	4.5	
2X Threshold to 120X Threshold	~ 2.5	
1.25 Threshold to 15X Threshold	~ 3.0	2.9
2X Threshold to 15X Threshold	~ 1.7	~ 1.0
Width Change with Input Amplitude Change (nsec)		
Threshold to 120X Threshold	2.6	
1.25X Threshold to 20X Threshold	~ 1.0	~ 1.0
Amplitude Change with Input Amplitude Change (%)		
Threshold to 120X Threshold	20	
1.25X Threshold to 20X Threshold	~ 7.5	27
Width Change with Temperature (%)		
0-120°F	+ 5	- 1.5
Amplitude Change with Temperature (%)		
0-120°F	+ 6	- 11

\*This is essentially a recapitulation of data previously given in the text, made for purposes of convenient comparison.

### 3. Coincidence and Anticoincidence Modules

#### 3.1. Slow-Recovery Coincidence Module

A circuit diagram of a slow-recovery coincidence module employing tunnel diode univibrators is shown in Fig. 25. Standardized pulses from each of three discriminators are added linearly at the input univibrator, which can be biased to trigger on a single pulse, on any two of three pulses, or on all three input pulses in coincidence. The three 50- $\Omega$  inputs are terminated by the 1:3 transformers, which also provide d-c isolation between modules. Since the input pulses from the discriminator are essentially triangular, the coincidence resolving time can be varied over several nsec (by the d-c bias adjustments shown) without single-pulse feed-through. Typical delayed-coincidence edges for pulses from a pulse generator are 0.1 nsec wide or less.

The behavior of this module with temperature is summarized in Table 2, which shows the results from temperature-cycling a dual input circuit.

Table 2. Response of Slow-Coincidence Module at Various Temperatures

Temperature (°F)	Half-Fire Point (nsec)		Resolution (nsec)
	Lower Pulse Edge	Upper Pulse Edge	
20	12.35	19.12	6.77
40	12.57	19.30	6.73
60	12.69	19.45	6.76
80	12.81	19.70	6.89
100	12.93	19.95	7.02
120	13.07	20.15	7.08

For a change in temperature from 20 to 120°F the variation in resolution is about 4%, while the change in edge timing is about 1 nsec.

UNCLASSIFIED  
ORNL-DWG 63-6095R

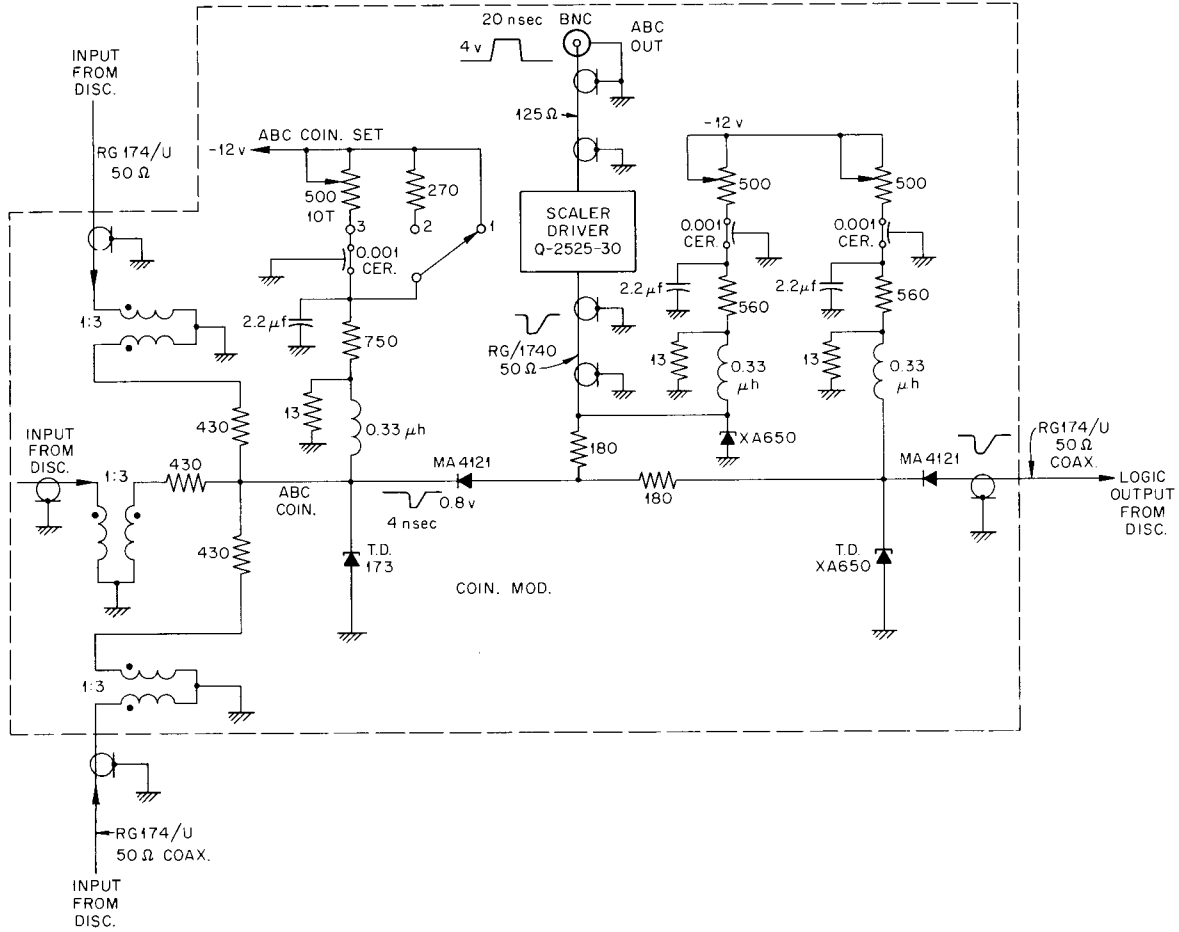


Fig. 25. Slow-Coincidence Module Circuit.

### 3.2. Fast-Recovery Coincidence Module

A circuit diagram of a fast-recovery coincidence module is shown in Fig. 26. As a comparison with Fig. 25 shows, the basic difference between the fast and slow modules is the use of nonlinear biasing (2N976). The fast-recovery coincidence module with a 2-nsec resolving time is capable of pulse-pair resolution of 10 nsec and has been so operated in accelerator proton beams with coincidence efficiencies in excess of 99%.

### 3.3. Anticoincidence Module

A circuit diagram of an anticoincidence module is shown in Fig. 27. The anticoincidence function is performed by a typical discriminator which feeds a modified scaler-driver module. The width of the scaler-driver pulse is accurately controlled by a 93- $\Omega$  shorted delay line. Two 10-nsec 4-V pulses with 4-nsec edges can be produced by this combination of modules within a period of 30 nsec, a resolution which is more than adequate for the resolution requirements ( $\leq 40$  nsec) of the experiments in which it is employed. The nonlinear biasing of the tunnel-diode univibrators in positions 1 and 2 permits the use of long-duration anticoincidence pulses without loss of sensitivity to the d-c portions of the pulse. In addition, the slight decrease in sensitivity to the fast edges of a pulse for this method of biasing helps to prevent the diodes from triggering on the back edge of the anticoincidence pulse.

## 4. Scaler-Driver Modules

At each logic step in the modules described above, a tunnel diode fanout output is provided for counting purposes. The nominal 1-V pulse of the gallium-arsenide tunnel diodes when used with an isolated coupling diode was insufficient for the reliable operation of commercially available scalars. For this reason, and to meet the requirement of  $\leq 40$ -nsec resolution, several scaler-driver modules were designed to drive scalars from either positive or negative tunnel-diode pulses.

### 4.1. Positive- and Negative-Output Scaler Drivers

The positive-output scaler driver, diagrammed in Fig. 28, delivers a 4-V pulse with 4-nsec edges into a 125- $\Omega$  load; the negative-output

UNCLASSIFIED  
ORNL-DWG 64-1189R

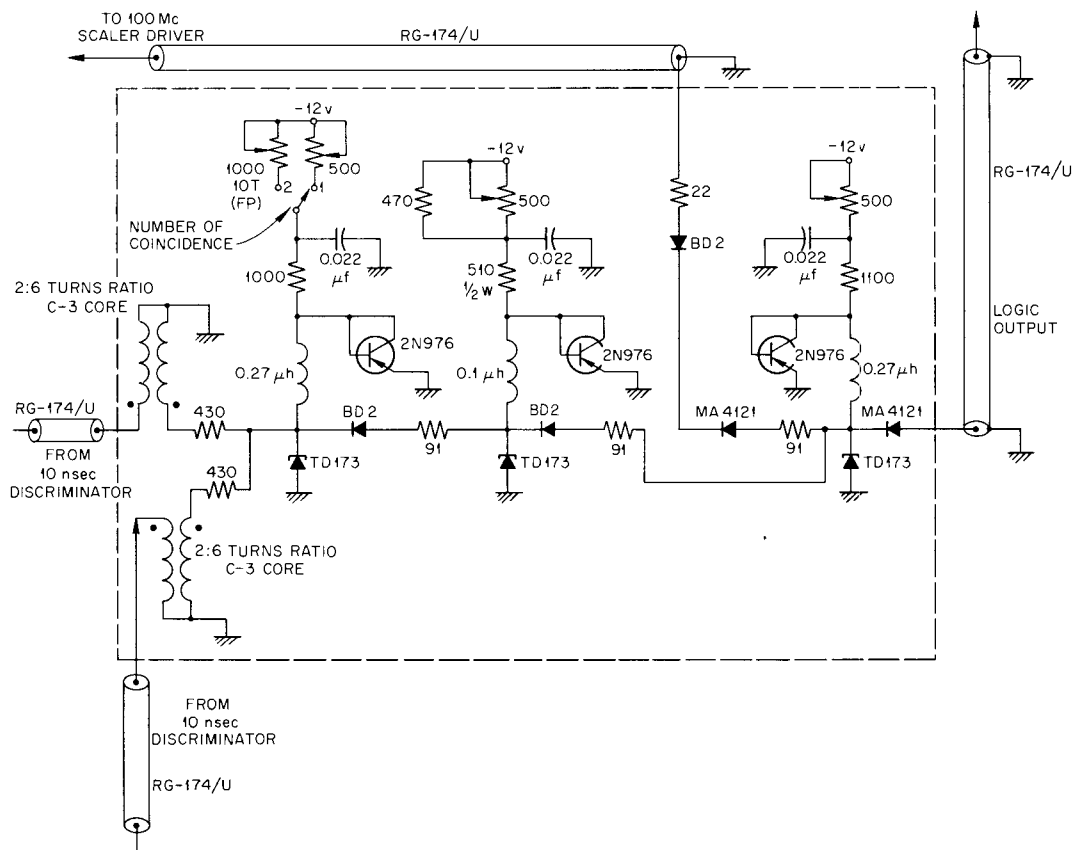


Fig. 26. Fast-Coincidence Module Circuit.

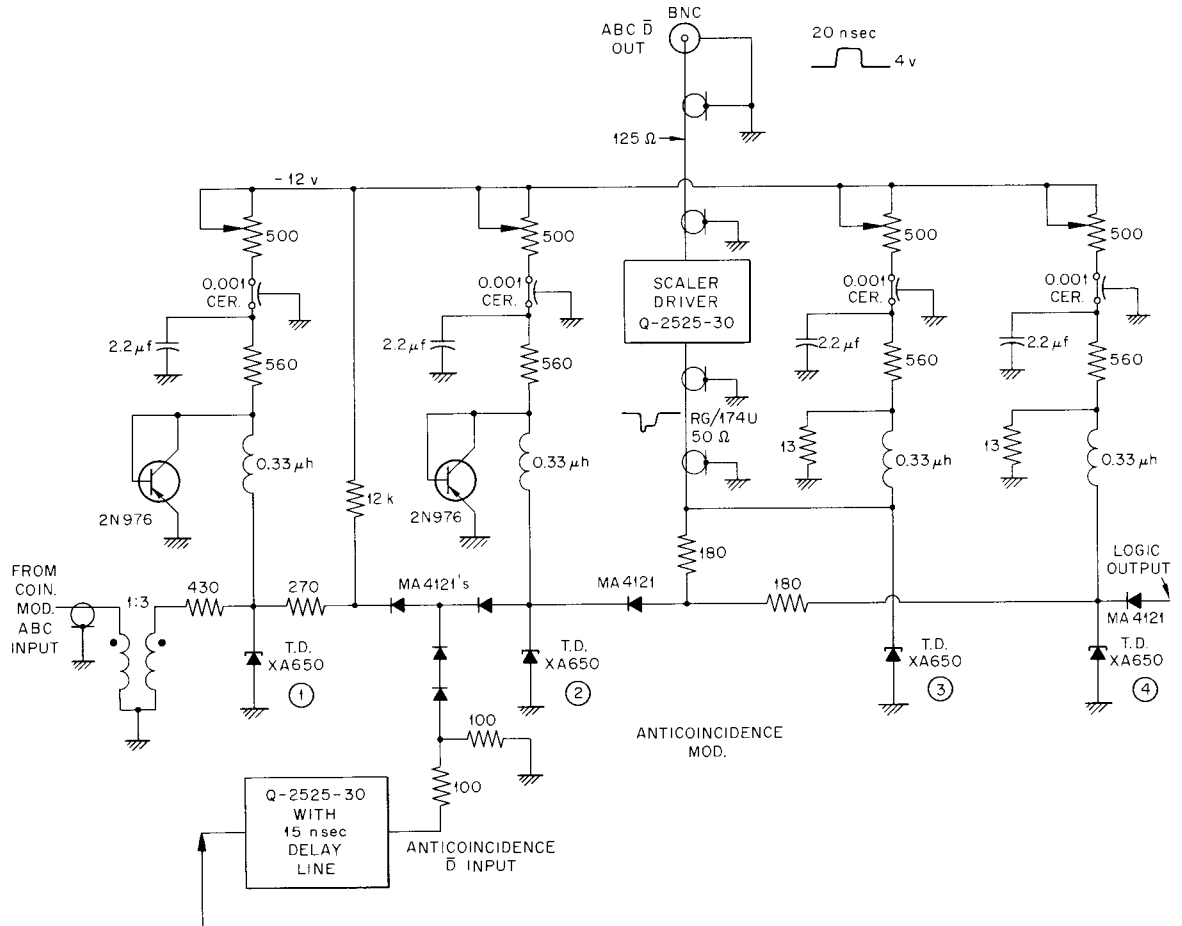


Fig. 27. Anticoincidence Module Circuit.



scaler driver, shown in Fig. 29, a 4-V pulse with 7-nsec edges into a 125- $\Omega$  load. Both have been operated with delay lines for accurate and stable output widths ranging from 10 to 90 nsec for use in logic functions such as those of the coincidence and anticoincidence modules. More commonly, however, the output-pulse widths have been controlled by the collector time constant in the trigger pair (see Figs. 28 and 29). The behavior of both positive- and negative-output scaler drivers with temperature is dependent upon the required output pulse width. For the positive-output driver operating without delay line width control, a temperature variation of 120°F produced a pulse widening of 19 nsec (0.16 nsec/°F) for a 60-nsec width at 75°F, and an amplitude increase of 2%. For a 490-nsec width at 75°F, the 120°F variation resulted in a widening of 53 nsec (0.44 nsec/°F) and an amplitude increase of 3.3%. The delay change over 120°F was 2.3 nsec, of which 0.3 nsec was due to discriminator walk. With delay line input the width change was 0.75 nsec over a 122°F range, for a 17-nsec width at 75°F, and the amplitude change was 2%.

The negative-output scaler driver without delay line width control showed a 13-nsec (0.11 nsec/°F) widening for a 50-nsec width at 75°F and a 120°F change, with an amplitude increase of ~ 7%. For a 460-nsec width at 75°F the widening was 92 nsec (0.77 nsec/°F) and the amplitude increase was ~ 7%. The delay change was 2.6 nsec, with 0.3 nsec due to discriminator walk. With delay line width control the result for a 122°F variation was a 1.0-nsec increase in width for an 18-nsec width at 75°F, and an amplitude change of 2.4%. At temperatures greater than 100°F a very slight negative slope appeared on the peak of the waveform.

Since more precise widths and amplitudes of the output pulses were not required, no attempt was made to provide additional temperature compensation for either scaler driver.

For both scaler drivers, with and without delay lines, the change in delay or walk with overdrive was observed to be dependent only on walk in the discriminator furnishing the input.

#### 4.2. 100-Mc Scaler Driver

The resolution demands ( ~ 10 nsec) of some of the experiments proposed could not be met with the scaler-driver modules described above.

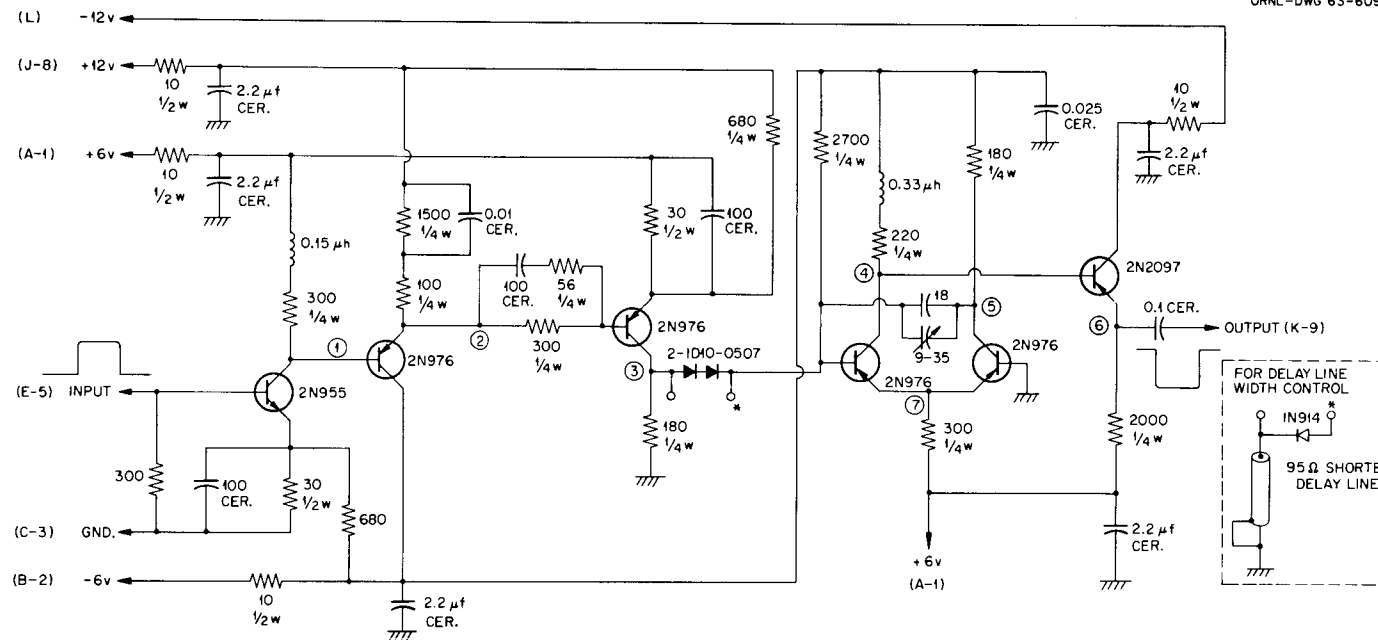


Fig. 29. Negative-Output Scaler-Driver Circuit.

To satisfy these needs the circuit shown in Fig. 30 was designed. It is capable, in conjunction with the nonlinearly loaded univibrators described earlier, of pulse quintuplicate resolution with 10-nsec spacing at a pulse train rate of 50 kc into a 50- $\Omega$  resistance, delivering a 3.5-V, 4-nsec-wide pulse.

The behavior of the 100-Mc scaler driver with temperature is shown in Fig. 31. As the figure shows, over a 90°F range in temperature, from 30 to 120°F, pulse width increases ~ 19%, pulse amplitude ~ 20%, and pulse rise time ~ 37%.

### 5. Scaler Modifications

In order to satisfy the resolution requirement for the counting equipment ( $\leq 40$  nsec), it was necessary to modify the input gate, limiter, and pulse shapers of the scalers<sup>14</sup> used in these experiments. The modifications are shown in the circuit diagram of Fig. 32. When this circuit is used with input A, the scaler has a pulse-pair resolution of less than 40 nsec for input pulses with widths ranging from 6 to 20 nsec and rise times ranging from 2 to 8 nsec. For a 15-nsec-wide pulse of either polarity the required input pulse amplitude is 1.5 V. A continuous counting rate greater than 12 Mc is possible, and pulse amplitudes in excess of 20 V can be tolerated and gated out. This circuit, however, does not respond to pulses having rise times slower than 1.5  $\mu$ sec; therefore input B was developed. Using input B the circuitry is capable of a pulse-pair resolution of less than 35 nsec for input pulses which have widths ranging from 6 to 20 nsec and rise times ranging from 2 to 8 nsec. Input B also allows operation in excess of 12 Mc and permits scaling sine-wave inputs well below 60 cps. (Amplitude requirements to scale sine waves down to 17 cps are less than 2.5 V/peak.)

### 6. Power Supply Regulation

Power supply fluctuations strongly affect timing and thresholds of the modules which have been described above. For the single test univibrator discussed in the early pages of this report, a change in the power-supply voltage produces a change in the threshold level, the change being a function of the threshold level. For example, if the threshold level is

14. Computer Measurements Corp. Model No. 1217A.

UNCLASSIFIED  
ORNL-DWG 63-6101

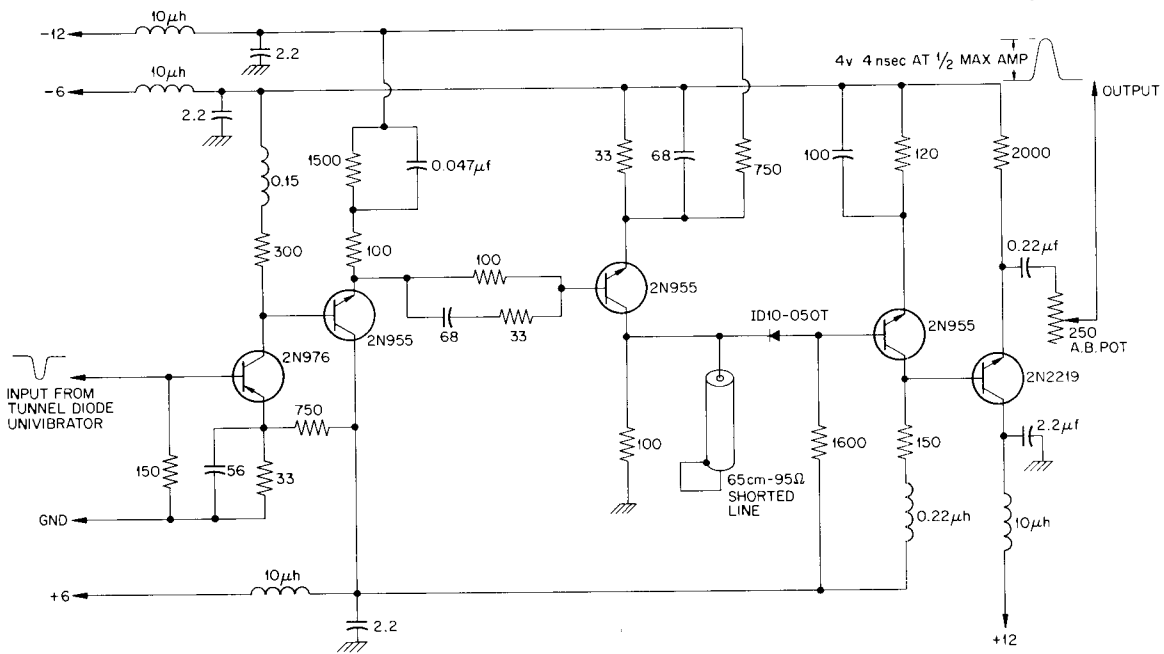


Fig. 30. Circuit for 100-Mc Scaler Driver.

UNCLASSIFIED  
ORNL-DWG 63-6102

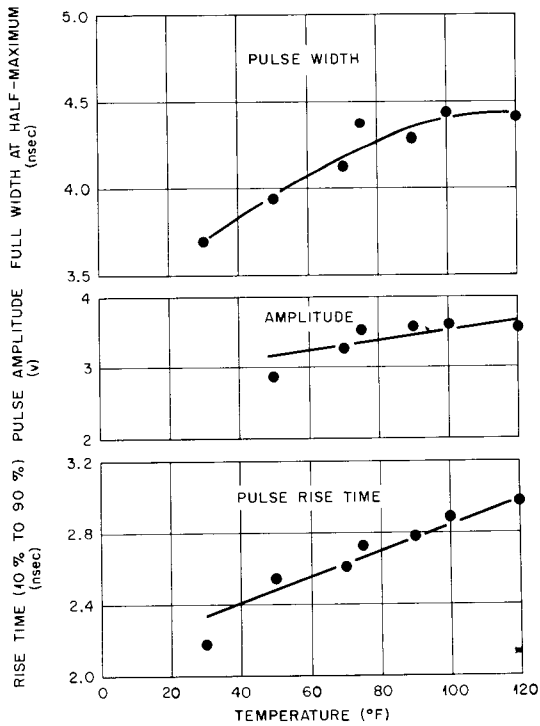


Fig. 31. Variation of Pulse Rise Time, Pulse Amplitude, and Pulse Width of 100-Mc Scaler Driver with Temperature.

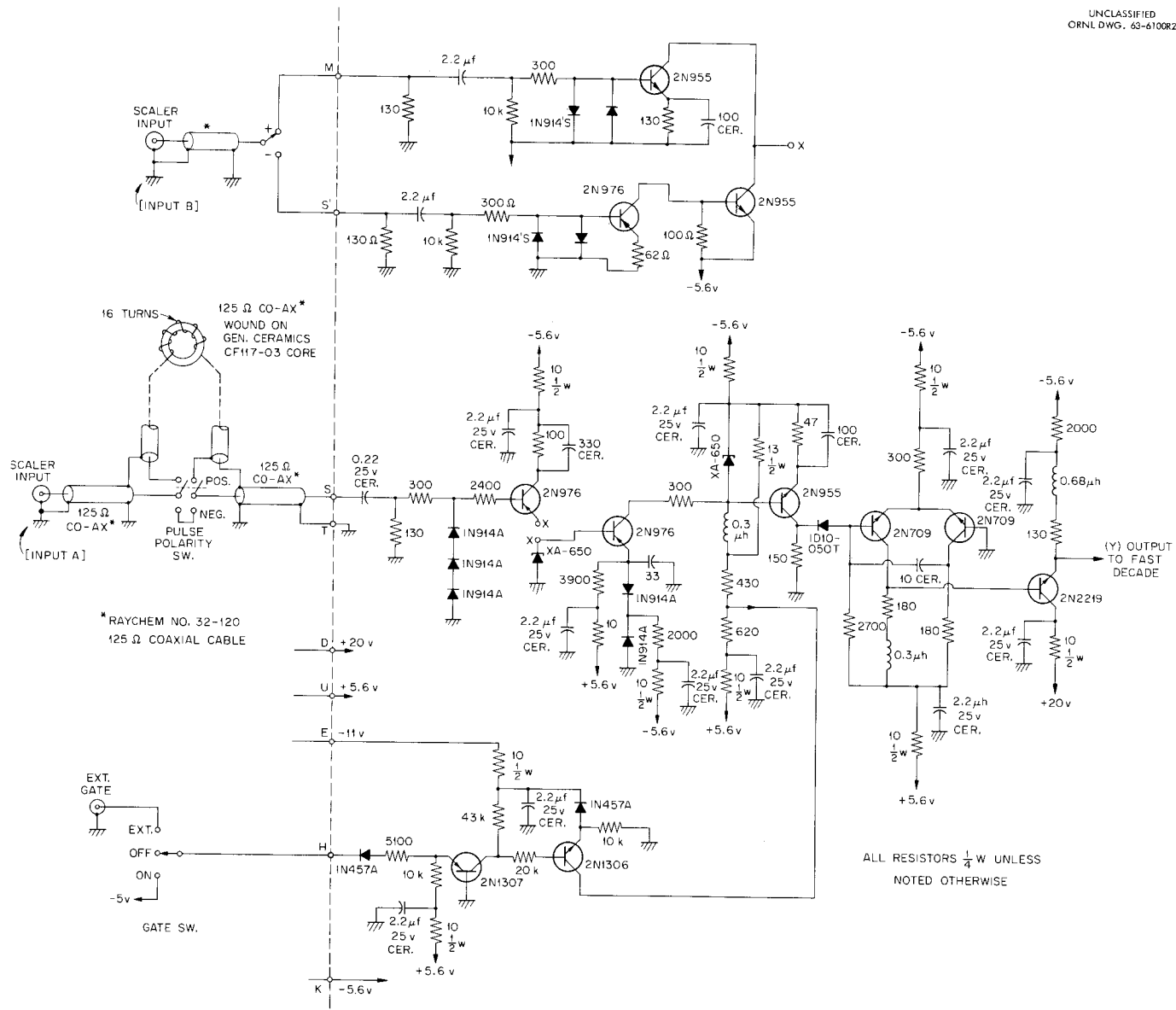


Fig. 32. Circuit Diagram Showing Modifications to CMC Scaler.

at 100  $\mu$ A of input current, a 0.1% increase in the power supply voltage lowers the threshold level by 2.3%. If the threshold is at 600  $\mu$ A, however, a 0.1% increase in the power supply voltage lowers the threshold level by only 0.9%.

When the univibrators are combined in modules the effects of power fluctuations are intensified. A slow-recovery discriminator whose threshold is  $\sim 0.4$  mA with a power supply of 12 V has its threshold changed by  $\sim \pm 0.05$  mA by a power supply change of  $\pm 1\%$ . This change of threshold represents a  $\pm 12\%$  change in drive requirements to the discriminator, and represents considerable walk when the discriminator is operating with inputs at or near threshold. For an input pulse having a rise time of  $< 1$  nsec and an amplitude of several times threshold, the walk as seen at the logic output of a slow-recovery discriminator was  $\sim 0.1$  nsec for a  $\pm 1\%$  power-supply voltage variation, with both tunnel diodes biased within 0.5 mA of their peak current point. When the logic output diode alone was adjusted to require a 2- to 3-mA drive, the  $\pm 1\%$  power-supply voltage variation caused a  $\sim 1.0$ -nsec change in output timing.

Because of the circuit's sensitivity to the trailing edge of the anticoincidence pulse, the numbers 1 and 2 diodes of the circuit shown in Fig. 27 must operate at biases of from 1 to 2 mA below their peak current point. Thus a  $\pm 1\%$  shift in power-supply voltage produces a  $\sim 0.6$  nsec change in output timing for this module.

Since these tunnel-diode modules are generally used in logic systems which form long series chains, the time shifts due to a  $\pm 1\%$  power variation are accumulative, amounting to 3.0 nsec for a typical logic system consisting of one discriminator and coincidence module and three anticoincidence modules. In view of the above, it is concluded that the power supply for the modules discussed in this report should be regulated to  $\pm 0.01\%$  for both line and load and be permitted a variation with temperature of not more than  $\pm 0.01\%/^{\circ}\text{C}$ . Ripple and noise should be less than 1 mV rms, particularly for the discriminators having 2-mV sensitivity.

### Appendix A. Construction Details

Generally the modules are constructed of double-sized printed circuit boards. After fabrication the 3-mil-thick copper cladding is gold-plated to a thickness of 0.1 mil or less, protecting the copper and permitting operation at frequencies in excess of 1 kMc without skin effect losses in the gold. In most cases the dielectric material is epoxy-filled fibre glass having a dielectric constant of from 4.7 to 5.

Signal paths, particularly for the faster electronics, have been made as double-sided strips with widths of  $3/32$  in. or greater, thus minimizing inductive effects. Double-sided copper ground sheets are fixed on both sides of the signal paths, providing isolation and an impedance close to the 50- $\Omega$  impedance associated with the cable used to interconnect the modules. No copper is unnecessarily etched from the boards and layouts are so made as to maintain continuous ground sheets. The sides of both signal paths and ground sheets are riveted together at regular intervals to prevent the formation of spurious signals.

The copper grounds and signal paths form the male half of the connection to a Viking 2VH6/1AN8 printed circuit connector, which was found to have low VSWR when used as a 50- $\Omega$  connection. Contact is made on both sides of the plug-in, reducing contact resistance and providing reasonable transmission lines for signals in 50  $\Omega$ . All panel coaxial connections are continued by coaxial cable to the connectors, thus effecting signal grounds at the most suitable points and maintaining equal signal delays for coincidence circuitry.

Direct-current power is supplied to the modules through ceramic feedthrough capacitors mounted on gold-plated copper bus bars, which in turn are mounted at the rear of the plug-in connectors. The bus bars serve as "dirty" grounds for bypassing power supply noise. Additional bypassing is accomplished on the modules themselves through the use of 2.2- $\mu$ F, 25-V ceramic capacitors mounted at the point which is to be bypassed. For tunnel diode circuits the length of the leads of such capacitors is limited to less than  $1/4$  in. All ground returns which carry signals, including

the bypass capacitors just mentioned, are grounded at a common point on the ground sheet. From this point a "clean" bus bar returns the ground to the power supplies.

Individual modules are mounted in the horizontal plane, edge to edge. This method minimizes stray coupling from module to module and permits easy inspection and servicing.

ORNL-3687  
 UC-37 - Instruments  
 TID-4500 (32nd ed.)

## INTERNAL DISTRIBUTION

- |                                     |                                   |
|-------------------------------------|-----------------------------------|
| 1. Biology Library                  | 45. T. A. Love                    |
| 2-4. Central Research Library       | 46. J. L. Lovvorn                 |
| 5. Reactor Division Library         | 47. J. M. Madison                 |
| 6-7. ORNL - Y-12 Technical Library  | 48. J. W. McConnell               |
| Document Reference Section          | 49. Ronald Nutt                   |
| 8-27. Laboratory Records Department | 50. R. Peelle                     |
| 28. Laboratory Records, ORNL R.C.   | 51. R. T. Santoro                 |
| 29. J. B. Ball                      | 52. M. J. Skinner                 |
| 30. R. Bender                       | 53. J. A. Swartout                |
| 31. R. D. Birkhoff                  | 54. J. R. Tarrent                 |
| 32. T. V. Blalock                   | 55. J. H. Thorngate               |
| 33. E. P. Blizard                   | 56. J. W. Wachter                 |
| 34. T. V. Blosser                   | 57. A. M. Weinberg                |
| 35. J. K. Dickens                   | 58. H. N. Wilson                  |
| 36. R. M. Freestone, Jr.            | 59. R. E. Whitt                   |
| 37. W. A. Gibson                    | 60. J. W. Woody, Jr.              |
| 38. K. M. Henry                     | 61. N. F. Ziegler                 |
| 39. N. W. Hill                      | 62. W. Zobel                      |
| 40. J. W. Johnson                   | 63. R. A. Charpie (consultant)    |
| 41. W. H. Jordan                    | 64. P. F. Gast (consultant)       |
| 42. W. E. Kinney                    | 65. M. L. Goldberger (consultant) |
| 43. C. E. Larson                    | 66. R. F. Taschek (consultant)    |
| 44. T. A. Lewis                     | 67. T. J. Thompson (consultant)   |

## EXTERNAL DISTRIBUTION

68. Lt. Duane Adams, Air Force Weapons Laboratory, WLRB-1, Kirtland Air Force Base, New Mexico
69. Lt. Col. R. G. Allen, Jr., USAF Aerospace Medical Center, Brooks Air Force Base, Texas
70. C. K. Bauer, Lockheed-Georgia Company, Marietta, Georgia
71. N. Barr, Chief, Radiological Physics Branch, Division of Biology and Medicine, AEC, Washington, D.C.
72. E. R. Beever, Space and Information Systems Division, North American Aviation, Inc., Downey, California
73. M. J. Berger, National Bureau of Standards, Washington, D.C.
74. S. Bresticker, Grumman Aircraft Engineering Corporation, Bethpage, Long Island, New York
75. Fred Casal, NASA Headquarters, Washington, D.C.
76. Mac C. Chapman, Northrop Space Laboratories, Hawthorne, California
77. T. H. Colvin, Nuclear Sciences and Space Power Department, Bendix Systems Division, Ann Arbor, Michigan
78. Col. J. Conner, Office of Advance Research and Technology, National Aeronautics and Space Administration, Washington, D.C.

79. Capt. R. F. Cooper, ASRPE-20, Wright-Patterson Air Force Base, Ohio
80. R. B. Curtis, University of Indiana, Bloomington, Indiana
81. C. A. Dempsey, 6570 AMRL, Wright-Patterson Air Force Base, Ohio
82. T. W. De Vries, General Dynamics, Fort Worth, Texas
83. Ed Divita, 1504 Doxbury Road, Towson, Maryland
84. D. L. Dye, Boeing Aircraft Company, Seattle, Washington
85. D. W. Drawbaugh, Westinghouse Electric Company, Pittsburgh, Pennsylvania
86. J. E. Duberg, NASA Langley Field, Virginia
87. F. Felberg, Jet Propulsion Laboratory, Pasadena, California
88. Trutz Foelsche, NASA Langley Research Center, Hampton, Virginia
89. R. E. Fortney, Northrop Space Laboratories, Hawthorne, California
90. E. M. Finkelman, Grumman Aircraft Engineering Corporation, Bethpage, Long Island, New York
91. Stan Freden, Aerospace Corporation, El Segundo, California
92. K. D. George, Reactor Requirements Office, Pictinny Arsenal, Dover, New Jersey
93. R. A. Glass, Lockheed Missiles and Space Company, Sunnyvale, California
94. R. V. Glowzowski, McDonnell Aircraft, St. Louis, Missouri
- 95-99. W. L. Gill, NASA Manned Spacecraft Center, Houston, Texas
100. R. C. Good, Jr., General Electric Company, Philadelphia, Pennsylvania
101. Lt. Col. Edward Harney, Air Force Space Systems Division, SSTA, Air Force Unit Post Office, Los Angeles, California
102. R. L. Harvey, General Electric Company, 175 Curtner Avenue, San Jose, California
103. W. N. Hess, Chief, NASA Theoretical Division, Goddard Space Flight Center, Greenbelt, Maryland
104. W. C. Hulten, NASA - IRD, Langley Research Center, Hampton Virginia
105. R. I. Hildebrand, Lewis Research Center, 21000 Brookpark Road, Cleveland, Ohio
106. C. W. Hill, Lockheed-Georgia Company, Marietta, Georgia
107. George Joanou, General Atomic, San Diego, California
108. Jim Johnson, LTV Research Center, Post Office Box 5003, Dallas, Texas
109. C. F. Johnson, General Dynamics/Fort Worth, Fort Worth, Texas
110. I. M. Karp, Lewis Research Center, Cleveland, Ohio
111. F. L. Keller, Aerospace Corporation, El Segundo, California
112. J. W. Keller, NASA Headquarters, Code RV-1, Washington, D.C.
113. J. F. Kenney, Boeing Scientific Research Laboratories, Seattle, Washington
114. M. R. Kinsler, North American Aviation, Inc., Space and Information Systems Division, Downey, California
115. Sol Krasner, Office of Naval Research, Washington, D.C.
116. E. C. Kidd, General Dynamics Corporation, Fort Worth, Texas
117. David Langford, Pratt and Whitney Aircraft, East Hartford, Connecticut
118. W. H. Langham, Los Alamos Scientific Laboratory, Los Alamos, New Mexico

119. Borje Larsson, The Gustaf Werner Institute, University of Uppsala, Uppsala, Sweden
120. L. R. Lewis, Nuclear Sciences and Space Power Department, Bendix Systems Division, Ann Arbor, Michigan
121. Martin Leimdorfer, Research Institute of National Defense, FOA4, Stockholm 80, Sweden
122. S. H. Levine, Northrop Space Laboratories, Hawthorne, California
123. Brian Mar, The Boeing Company, Seattle, Washington
124. R. J. Macklin, Jr., Jet Propulsion Laboratory, Pasadena, California
125. R. V. Meghreblian, Jet Propulsion Laboratory, Pasadena, California
126. R. A. Miller, General Dynamics, Fort Worth, Texas
127. Phil Mittleman, United Nuclear Corporation, White Plains, New York
128. Keith More, Bendix Systems Division, Ann Arbor, Michigan
- 129-153. Winnie M. Morgan, Office of Space Sciences, National Aeronautics and Space Administration, Washington, D.C.
154. J. L. Modisette, Space Environment Division, Manned Spacecraft Center, Houston, Texas
155. T. J. McGuire, ASD(ASRSSV-e), Shielding Research Reports, ASR55-54, Wright-Patterson Air Force Base, Ohio
156. L. W. McCleary, Space and Information Systems Division, North American Aviation, Inc., Downey, California
157. J. C. Noyes, Boeing Scientific Research Laboratories, Seattle, Washington
158. J. P. Neissel, General Electric Company, Schenectady, New York
159. Richard Madey, Republic Aviation Corporation, Farmingdale, Long Island, New York
160. Wade Patterson, University of California Radiation Laboratory, Berkeley, California
161. Maynard Pearson, The Boeing Company, Seattle, Washington
162. G. F. Pieper, NASA Headquarters, Greenbelt, Maryland
163. Robert Pruet, Aerospace Corporation, El Segundo, California
164. Loren Pittman, 6570 AMRL (MRBBR), Wright-Patterson Air Force Base, Ohio
165. Col. J. E. Pickering, USAF Aerospace Medical Center, Brooks Air Force Base, Texas
166. Frederick Raymes, North American Aviation, Inc., Downey, California
167. Arthur Reetz, NASA Headquarters, Washington, D.C.
168. Evalyn Repplinger, Crew Systems Division, Post Office Box 1537, Houston, Texas
- 169-173. O. Reynolds, Director, Office of Space Sciences, National Aeronautics and Space Administration, Washington, D.C.
174. General C. Roadman, Director, Office of Manned Space Flight, National Aeronautics and Space Administration, Washington, D.C.
175. D. H. Robey, General Dynamics/Astronautics, San Diego, California
176. Sidney Russak, The Martin Company, Baltimore, Maryland
177. T. J. Rock, General Dynamics/Fort Worth, Fort Worth, Texas

178. Hermann Schaefer, U.S. Naval Aviation Medical Center-54, Pensacola, Florida
179. F. E. Schwamb, Republic Aviation Corporation, Farmingdale, Long Island, New York
180. H. J. Schulte, Bellcomm, Inc., Washington, D.C.
181. W. M. Schofield, Advanced Research Corporation, 3127 Maple Drive, Atlanta, Georgia
- 182-186. R. J. Scroggs, Oak Ridge Technical Enterprises Corporation, Oak Ridge, Tennessee
187. S. P. Shen, New York University, New York, New York
188. E. C. Smith, Advanced Research Corporation, 3127 Maple Drive, Atlanta, Georgia
189. G. D. Smith, Ames Research Center, Moffett Field, California
190. Jerry Speakman, 6570 AMRL (MRBBR), Wright-Patterson Air Force Base, Ohio
191. Dwaine F. Spencer, Jet Propulsion Laboratory, Pasadena, California
192. R. T. Stiegel, College of William and Mary, Williamsburg, Virginia
193. R. H. Steelle, NASA Manned Spacecraft Center, Houston, Texas
194. H. E. Stern (M-RP-N), George C. Marshall Space Flight Center, Huntsville, Alabama
195. T. R. Strayhorn, General Dynamics, Fort Worth, Texas
196. William Steigelmann, Kuljian Corporation, 1200 North Broad Street, Philadelphia, Pennsylvania
197. Cornelius Tobias, University of California Radiation Laboratory, Berkeley, California
198. M. A. Van Dilla, Los Alamos Scientific Laboratory, Los Alamos, New Mexico
199. L. F. Vosteen, NASA Langley Research Center, Hampton, Virginia
200. Frank Voorhis, USAF (MC), OART/RBH, NASA, Washington, D.C.
201. F. Voris, Office of Advanced Research and Technology, National Aeronautics and Space Administration, Washington, D.C.
202. G. P. Wachtell, Franklin Institute, 20th and Parkway, Philadelphia, Pennsylvania
203. G. T. Western, General Dynamics/Fort Worth, Fort Worth, Texas
204. G. A. Whan, University of New Mexico, Albuquerque, New Mexico
205. Maurice Wilkinson, The Boeing Company, Seattle, Washington
206. Clayton Zerby, Union Carbide Research Institute, Tarrytown, New York
207. K. Ziock, University of Virginia, Charlottesville, Virginia
208. Research and Development Division, AEC, ORO
- 209-845. Given distribution as shown in TID-4500 (32nd ed.) under Instruments category (100 copies - OTS)